DOI: 10.1002/ejic.201100630

Helical Complexes of Chiral Quaterpyridines – Mononuclear Cu^{II} and Dinuclear Cu^{I} Complexes

Ho-Lun Yeung,[a] Kiu-Chor Sham,[a] Wai-Yeung Wong,[b] Chun-Yuen Wong,*[a] and Hoi-Lun Kwong*[a]

Keywords: Copper / Helical structures / Quaterpyridine ligands / Circular dichroism

Two series of chiral helical copper–quaterpyridine complexes were prepared by reacting chiral ligands **L1**–**4** with Cu^{I} and Cu^{II} precursors. The Cu^{II} complexes, $[Cu(\mathbf{L})(H_2O)(ClO_4)_2]$ or $[Cu(\mathbf{L})(ClO_4)_2]$, were studied by ESI-MS, elemental analysis, and CD spectroscopy, and the Cu^{I} complexes, $[Cu_2(\mathbf{L})_2](PF_6)_2$, were examined by NMR, ESI-MS, elemental analysis, and CD spectroscopy. The crystal structures of $[Cu(\mathbf{L1})(H_2O)(ClO_4)](ClO_4)$ and $[Cu(\mathbf{L3})(ClO_4)_2]$ were determined by X-ray diffraction. They are monomeric, distorted octahedral complexes with the quaterpyridine ligand coordinated at the four equatorial positions and one or two perchlorates at the apical position. The crystal structure of $[Cu(\mathbf{L1m})(H_2O)(ClO_4)](ClO_4)$, which has an achiral quaterpyridine ligand **L1m**, the *meso* form of **L1**, was also determined. Comparison between $[Cu(\mathbf{L1})(H_2O)(ClO_4)](ClO_4)$ and $[Cu(\mathbf{L1m})(H_2O)(ClO_4)](ClO_4)$ shows small differences between the two structures. CD analyses of mononuclear Cu^{II} complexes of sterically demanding **L2**–**4** indicate that these structures require a helical twist in the ligand. The crystal structure of $[Cu_2(\mathbf{L3})_2](PF_6)_2$ shows that it is a two-metal two-ligand double-stranded helical structure. Solution NMR studies of the dinuclear Cu^{I} complexes show that each sample consists of two diastereomers with moderate to high diastereoselectivity (52–99 %). With **L1m**, head-to-head and head-to-tail configurational isomers were formed in an almost 1:1 ratio. Heterostranded helicates could also be formed with two different chiral ligands but selectivity favors the homostranded one. DFT calculations on the homostranded helicates yield evidence that interactions between the chiral groups of the ligand strands in the helicate are not solely responsible for determining the helical chirality of the Cu^{I} complexes.

Introduction

Helical metal complexes, both mononuclear and polynuclear, have fascinated chemists since their discovery.[1,2] Although mononuclear varieties represent the basic unit with high asymmetry, polynuclear helicates are especially important for their role as benchmarks for the self-organization processes of supramolecular metal complexes.[3–5] Although helical metal complexes are chiral, they usually appear only as a racemic mixture when achiral ligands are used. The stereoselective formation of chiral helical complexes, which represents a higher hierarchical level of selective synthesis of metal complexes, is a challenge.[6] Indeed, recently the transfer of chirality from chiral nonracemic ligands to metal centers with a variety of coordination geometries has attracted great interest.[7] Applications of chiral helical metal complexes in various areas such as asymmetric catalysis,[8] DNA binding,[9] supramolecular functional devices,[10] and host–guest interactions[11] have started to emerge.

2,2′:6′,2″:6″,2‴-Quaterpyridine (qtpy), a tetradentate ligand, can form metal complexes of different geometries. Its versatility, variously demonstrated by Lehn,[12] Constable,[13] Potts,[14] and Che,[15] principally derives from the number of possible coordination modes of the ligand,

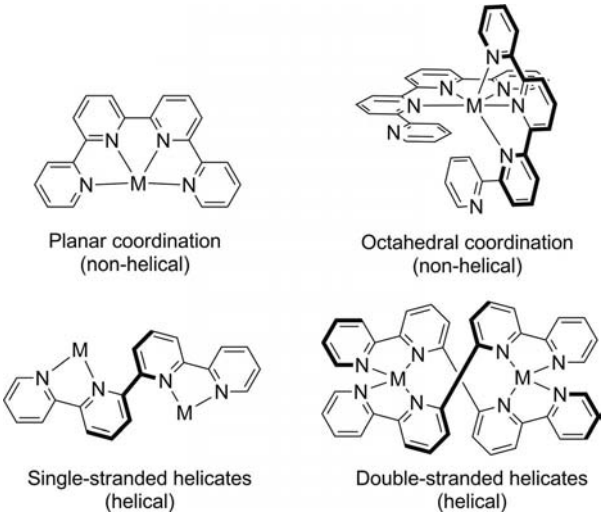

Scheme 1. Various coordination geometries of qtpy with metal ions.

[a] Department of Biology and Chemistry, City University of Hong Kong,
Tat Chee Avenue, Kowloon, Hong Kong SAR, China
[b] Department of Chemistry, Hong Kong Baptist University, Waterloo Road, Hong Kong SAR, China

Supporting information for this article is available on the WWW under http://dx.doi.org/10.1002/ejic.201100630.

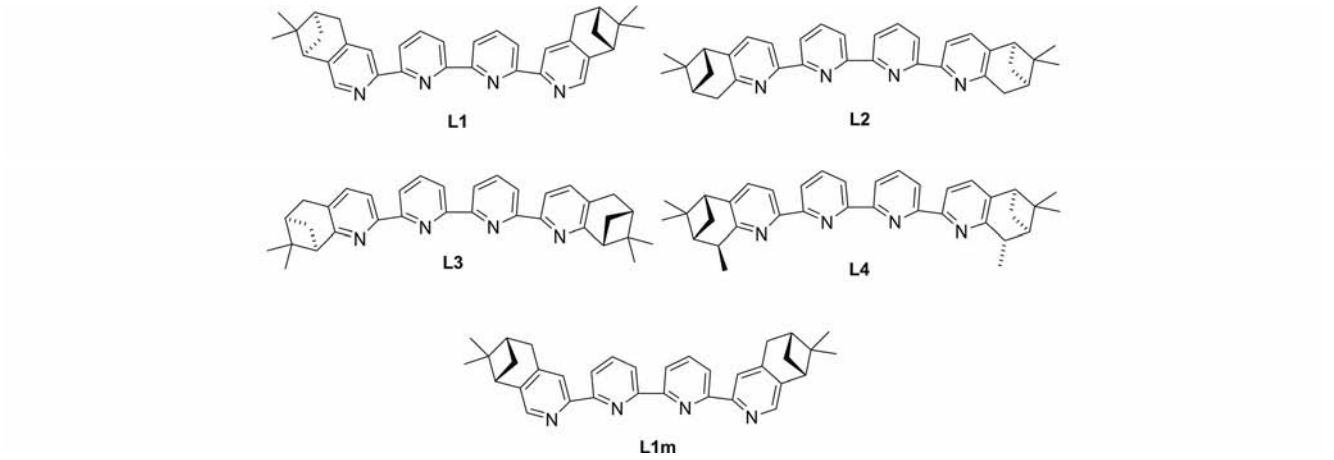

which readily possesses bi-, ter-, and tetradentate domains (Scheme 1). The majority of coordinated qtpy ligands behave in a near-planar fashion upon tetradentate complexation with square-planar and octahedral complexes, although a rare case of terdentate coordination in $[Fe(qtpy)_2]^{2+}$ has been reported.[16] Constable and coworkers have developed a series of substituted qtpy ligands to study the directional isomerism (head-to-head and head-to-tail) of double-stranded helicates.[17] They have reported the first chiral qtpy ligand (**L2** in this study), which induced high stereoselectivity in double-stranded helicates with tetrahedral d^{10} metal ions.[18]

Of all the transition metals, copper has a particular appeal because of the different stereoelectronic preferences of its two common oxidation states. This difference is due to the pronounced geometric change from the four-coordinate tetrahedral shape to a combination of five- or six-coordinate geometry. The geometric change at the metal center, with a suitable multidentate ligand, yields metal complexes with different topologies and distinct properties.[19,20] We have recently reported helical metal complexes of chiral oligopyridines.[21–23] Continuing our efforts to study the stereoselective formation of helical metal complexes, we present the stereoselective formation of single-stranded mononuclear Cu^{II} and double-stranded dinuclear Cu^{I} complexes with a series of simple, versatile chiral qtpy ligands, **L1**–**4**.

Results and Discussion

Ligand Synthesis and Characterization

Chiral **L1**–**4** were readily prepared by a three-step procedure, which we have reported previously.[22–24] NMR studies show that the crude qtpy ligands are always accompanied by a small amount of another compound during synthesis. For example, in the ^{1}H NMR spectrum of crude **L3**, a subset of resonances that constitute about 7% of the major compound can be observed at δ = 7.55, 7.78, 8.13, 8.35, and 8.48 ppm (Figure 1). Similar observations were made in the spectra of other crude qtpy ligands. An X-ray crystallographic study of a Cu^{II} complex obtained from the reaction of crude **L1** with Cu^{II} perchlorate confirms that the minor compound is the *meso* form of **L1** (**L1m**).

As the formation of **L1m** can be rationalized in terms of coupling between two enantiomers of the chiral bipyridine intermediate, the optical purity of commercially available

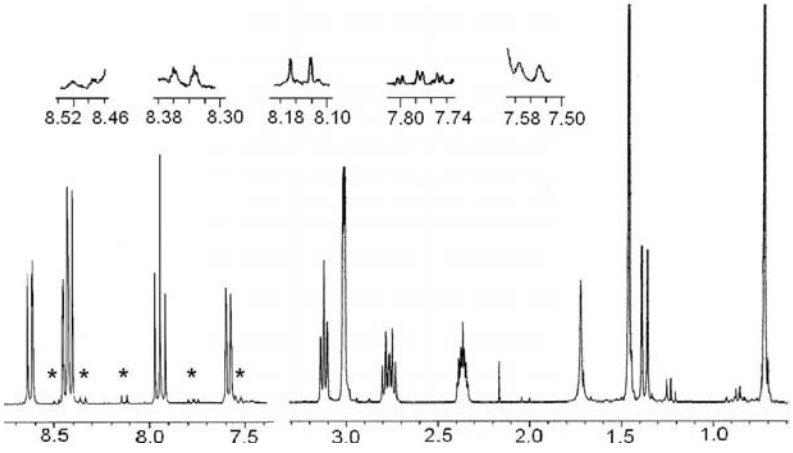

Figure 1. ^{1}H NMR spectrum of crude **L3** showing the presence of the minor compound, indicated by asterisks *. The insets shown peaks due to a minor compound.

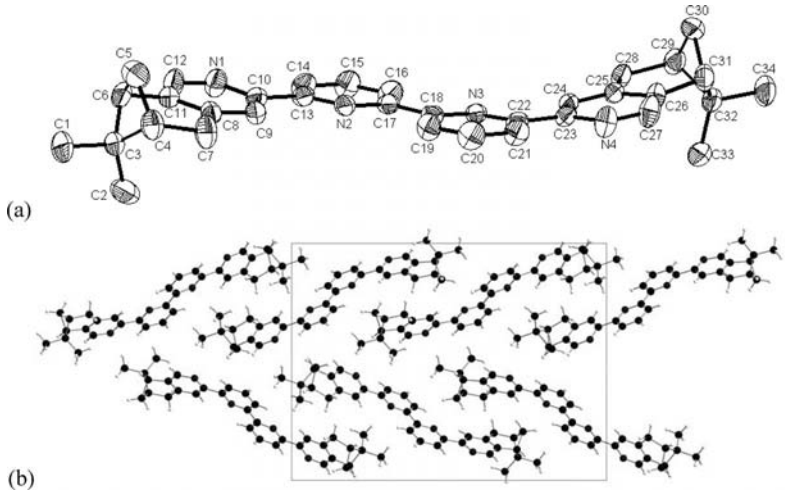

Figure 2. (a) ORTEP drawing of **L1** with atom labeling scheme and (b) packing diagram of **L1** in the crystal lattice viewed along the *a* axis.

myrtenal was analyzed by chiral GC to confirm the source of the minor enantiomer. The *ee* was found to be 93%, whereas that of other commercial terpenoid compounds (starting materials for **L2**–**4**) varied from 93–95%. Assuming a statistical distribution of coupled products, the amount of *meso* ligand can be estimated to be 5–7%, which is consistent with NMR studies of the crude ligands. As **L1**–**4** and their corresponding *meso* ligands are diastereomers with different solubilities, the *meso* ligands were removed by recrystallization. The acid salts of **L1**–**4**, formed from qtpy and HCl (6 N), were used for this purpose and were recrystallized from methanol. After treatment with 2 M NaOH, the desired ligands were obtained as white solids. Purified **L1**–**4** were then characterized again by ^{1}H NMR, which confirmed that they contained only one isomer.

After single crystals of enantiomerically pure **L1** were obtained by evaporation of a concentrated solution of **L1** in CH_2Cl_2, the solid-state structure was studied by X-ray crystallography. In the crystal structure, the pyridine rings adopt the expected *transoid* geometry (Figure 2, a), which is the same as 2,2′-bipyridine and 2,2′:6′,2′′:6′′,2′′′-qtpy. The bond lengths within the molecule closely approximate those observed in achiral qtpy. The torsion angles between the four pyridine rings are approximately *trans* coplanar [∠ N(1)–C(10)–C(13)–N(2): 173.2°; ∠N(2)–C(17)–C(18)–N(3): –179.0°; ∠N(3)–C(22)–C(23)–N(4): 176.2°]. In this respect, the molecule is slightly perturbed by the chiral auxiliaries. In the crystal packing, the molecules adopt a herringbone array with an interplanar separation of 6.69 Å and show no significant π–π interactions (Figure 2, b).

Synthesis and UV Characterization of Mononuclear Cu^{II}–qtpy Complexes

Complex formation of chiral qtpy was first examined with Cu^{II} (Scheme 2). Mononuclear Cu^{II} complexes were obtained by reacting equimolar amounts of enantiopure qtpy and hydrated $Cu(ClO_4)_2$ in methanol at room temperature. Instant color changes to blue or green-blue were observed with **L1**–**4**. After workup, the stoichiometries of the Cu^{II} complexes were established by combining elemental analyses and MS. All complexes have a 1:1 ligand:metal ratio and show major peaks of $[M - ClO_4^-]^+$ in the ESI-MS. The NMR spectra all show broad signals with strong paramagnetic peak shifts due to the d^9 Cu^{II} center. Achiral $[Cu(\mathbf{L1m})(H_2O)(ClO_4)](ClO_4)$, which was obtained as minor product from the complexation of Cu^{II} with crude **L1**, was also isolated as a pure crystalline solid.

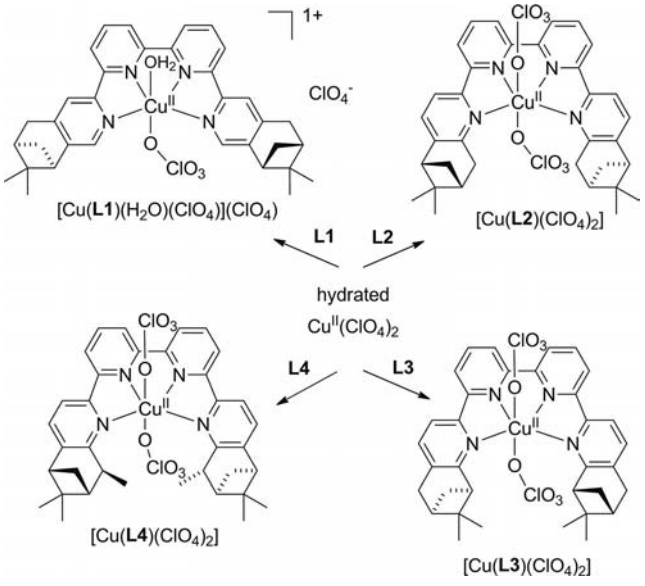

Scheme 2. Synthesis of mononuclear single-stranded Cu^{II} complexes with enantiopure **L1**–**4**.

The electronic absorption spectra of the Cu^{II} complexes are shown in Figure 3. The band maxima (λ_{max}) and molar absorptivities (ε) from these electronic spectra are presented in Table 1. In general, the UV region of the spectra is dominated by intense intraligand π–π* transitions. The transi-

tions in the visible region (550–900 nm) are attributed to weak *d*–*d* transitions. The absorption at 640 nm of [Cu(**L1**)-$(H_2O)(ClO_4)](ClO_4)$ falls within the typical blue region of octahedral Cu^{II} complexes. For $[Cu(\mathbf{L2})(ClO_4)_2]$, [Cu(**L3**)-$(ClO_4)_2]$, and $[Cu(\mathbf{L4})(ClO_4)_2]$, λ_{max} shifts towards longer wavelengths (90–134 nm). These very large shifts can be accounted for by the serious distortion imposed on the ideal octahedral coordination geometry.[12b,14c]

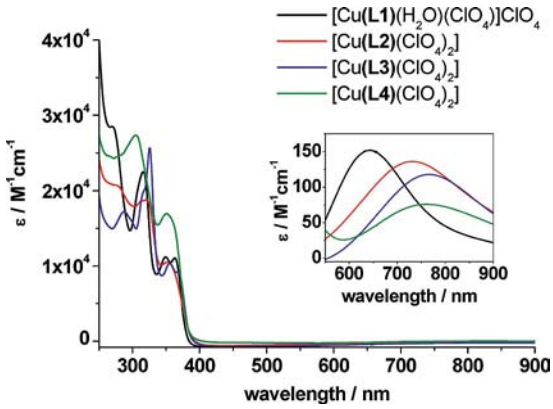

Figure 3. Electronic absorption spectra of mononuclear Cu^{II} complexes of **L1**–**4** at a concentration of 2.5×10^{-5} M at room temperature. Inset is shown the visible region (550–900 nm) at a concentration of 1×10^{-3} M.

Table 1. Electronic absorption spectroscopic data for Cu^{II} complexes of **L1**–**4** in CH_2Cl_2.

Complex	λ_{max} [nm] (ε/M^{-1} cm^{-2})
$[Cu(\mathbf{L1})(H_2O)(ClO_4)](ClO_4)$	315 (22.5×10^3), 349 (11.2×10^3), 363 (11.1×10^3), 640 (1.5×10^2)
$[Cu(\mathbf{L2})(ClO_4)_2]$	321 (18.8×10^3), 354 (10.3×10^3), 730 (1.4×10^2)
$[Cu(\mathbf{L3})(ClO_4)_2]$	325 (25.6×10^3), 356 (10.3×10^3), 369 (9.1×10^3), 764 (1.2×10^2)
$[Cu(\mathbf{L4})(ClO_4)_2]$	306 (27.3×10^3), 354 (16.8×10^3), 759 (8.0×10)

X-ray Structures of Cu^{II}-qtpy Complexes

Crystals of $[Cu(\mathbf{L1})(H_2O)(ClO_4)](ClO_4)$, [Cu(**L1m**)-$(H_2O)(ClO_4)](ClO_4)$, and $[Cu(\mathbf{L3})(ClO_4)_2]$ were obtained by slow evaporation of ethanolic solutions. ORTEP diagrams and space-filling models emphasizing the secondary structure of the ligand are shown in Figure 4. Selected bond lengths and angles are summarized in Table 2. Both [Cu-$(\mathbf{L1})(H_2O)(ClO_4)](ClO_4)$ and [Cu(**L1m**)$(H_2O)(ClO_4)](ClO_4)$ crystallized as blue blocks in a $P\bar{1}$ space group. The coordination geometries of the two mononuclear Cu centers are similar and exhibit a distorted octahedral geometry with four pyridine N donors coordinated at the equatorial positions and one water molecule and one perchlorate ligand coordinated at the axial positions. The average metal–nitrogen bond length involving the terminal rings (2.017 Å) is longer than that with the internal rings (1.932 Å). The dihedral angles between the terminal pyridine rings are 119.8 (3)° and 118.9 (2)°. In $[Cu(\mathbf{L1})(H_2O)(ClO_4)](ClO_4)$, **L1** of is almost coplanar; with only the third and fourth pyridine rings having a small torsion angle of 6.2°. The Cu^{II} complex of **L1m** shows an overall twist of 1.7° as a result of flipping between the pyridyl rings: 4.86° between the first and second pyridine rings, –6.31° between the second and third, and –0.28° between the third and fourth. Neither of the structures suffers from severe helical distortion. The closest H···H and C···C distances between the two chiral groups of $[Cu(\mathbf{L1})(H_2O)(ClO_4)](ClO_4)$ and [Cu(**L1m**)$(H_2O)(ClO_4)]$-(ClO_4) are 5.16 Å and 6.74 Å, and 5.18 and 6.77 Å, respectively.

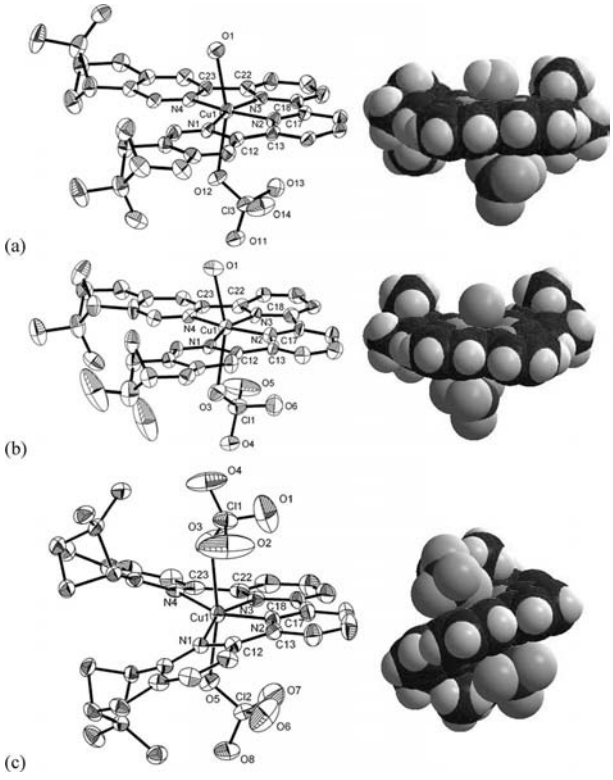

Figure 4. ORTEP drawings (showing partial labeling scheme) and space-filling models (emphasizing the ligand secondary structure) of (a) $[Cu(\mathbf{L1})(H_2O)(ClO_4)](ClO_4)$, (b) [Cu(**L1m**)$(H_2O)(ClO_4)]$-$(ClO_4)$, and (c) $[Cu(\mathbf{L3})(ClO_4)_2]$. Thermal ellipsoids are drawn at 30% probability. Hydrogen atoms are omitted for clarity.

In the crystal structure of $[Cu(\mathbf{L3})(ClO_4)_2]$, four pyridine N donors of the ligand and two perchlorate ligands are coordinated to the Cu^{II} ion in a distorted octahedral geometry. Due to the close proximity of two bulky chiral groups (closest H···H distance of 2.35 Å and C···C distance of 3.14 Å), the ligand is nonplanar. In minimizing the steric repulsion, the four pyridine rings are arranged in a helical conformation, with the first and the last pyridine rings flipping downwards and upwards, respectively, with an overall helical twist of 12.1°. The dihedral angles between the first and second, second and third, and third and fourth pyridine rings are 5.1, 2.6, and 4.4°, respectively. The N1–Cu–N4 dihedral angle [125.0 (1)°] and the corresponding Cu–N distances of terminal pyridine (2.098–2.100 Å) are significantly larger than those of the Cu^{II} complexes of **L1** and **L1m**,

Table 2. Selected X-ray data of mononuclear Cu^{II} complexes of **L1**, **L1m**, and **L3**.

	[Cu(**L1**)-$(H_2O)(ClO_4)](ClO_4)$	[Cu(**L1m**)-$(H_2O)(ClO_4)](ClO_4)$	Cu(**L3**)-$(ClO_4)_2$
Selected distances [Å]			
Cu–N1	2.039(6)	2.003(9)	2.098(3)
Cu–N2	1.937(7)	1.905(8)	1.954(3)
Cu–N3	1.936(5)	1.925(1)	1.951(3)
Cu–N4	2.033(6)	2.060(7)	2.100(3)
Cu–O(water)	2.406(6)	2.402(8)	–
Cu–O(perchlorate)	2.546(5)	2.572(8)	2.473(4), 2.523(3)
Selected angles [°]			
N1–C12–C13–N2	–0.4(9)	4.9(1)	5.1(4)
N2–C17–C18–N3	4.1(9)	–6.3(1)	2.6(5)
N3–C22–C23–N4	–3.3(9)	–0.3(1)	4.4(4)
Overall helical twist	0.4	–1.7	12.1

which is evidence that the steric repulsion established from the chiral groups of the ligand is stabilized by long Cu–N distances. The solid-state structure reveals the stereoselective formation of a *P*-helix.

CD Characterization of Cu^{II}–qtpy Complexes

CD experiments on the mononuclear Cu^{II} complexes were carried out in CH_2Cl_2 at room temperature (Figure 5). At a concentration of 1.32×10^{-5} M, the CD spectrum of $[Cu(\mathbf{L1})(H_2O)(ClO_4)](ClO_4)$ shows a very weak absorption ($\Delta\varepsilon$ = 5.2 $M^{-1}cm^{-1}$) in the region of 290–400 nm. This suggests that there is only weak secondary structure of $[Cu(\mathbf{L1})(H_2O)(ClO_4)](ClO_4)$ in solution. In contrast, $[Cu(\mathbf{L3})(ClO_4)_2]$ exhibits a strong sinoidal curve, with a larger positive amplitude at 371 nm ($\Delta\varepsilon$ = 34.1 $M^{-1}cm^{-1}$) and a weaker negative amplitude at 327 nm ($\Delta\varepsilon$ = 28.8 $M^{-1}cm^{-1}$). We believe that this bisignate curve originates from the π–π* bipyridine intraligand transitions.[25,26] This strong absorption (Cotton effect) indicates that the helical structure, as observed from the crystal structure, is retained in solution and, more significantly, it is consistent with the exciton chirality determined from the dihedral angles between the long-axes of the bipyridine units. Although $[Cu(\mathbf{L2})(ClO_4)_2]$ and $[Cu(\mathbf{L4})(ClO_4)_2]$ also show strong CD absorptions ($\Delta\varepsilon$ = 25.1 and 25.4 $M^{-1}cm^{-1}$, respectively), the signals are not as strong those of $[Cu(\mathbf{L3})(ClO_4)_2]$. On the basis of the crystal structure and theoretical models (vide infra), $[Cu(\mathbf{L2})(ClO_4)_2]$ is assigned as an *M*-helix, whereas $[Cu(\mathbf{L3})(ClO_4)_2]$ and $[Cu(\mathbf{L4})(ClO_4)_2]$ are assigned as *P*-helices.

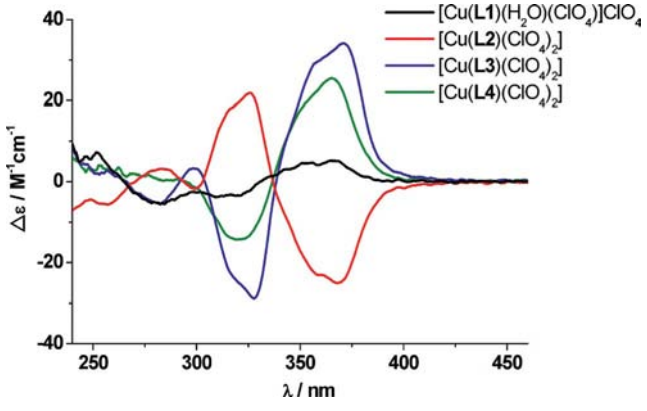

Figure 5. CD spectra of Cu^{II} complexes of **L1**–**4** in CH_2Cl_2 solutions.

Stereoselectivity and Molecular Modeling Study of Cu^{II}-qtpy Complexes

To understand the helicity and stereoselectivity of Cu^{II}–qtpy complexes, the structures of $[Cu(\mathbf{L})]^{2+}$ (**L** = **L1**–**4**) were modeled by DFT calculations (see detailed geometries in the Supporting Information). The simulation method was based on optimizing the geometry of the Cu^{II} complex for the lowest energy. With regard to bond lengths, bond angles, and metal geometries, the modeled structures of $[Cu(\mathbf{L1})]^{2+}$ and $[Cu(\mathbf{L3})]^{2+}$ closely resemble the corresponding crystal structures of $[Cu(\mathbf{L1})(H_2O)(ClO_4)](ClO_4)$ and $[Cu(\mathbf{L3})(ClO_4)_2]$. The four simulated structures have absolute configurations that are in agreement with the results of the CD experiments. For example, the four pyridyl rings in $[Cu(\mathbf{L1})]^{2+}$ are essentially coplanar, which is consistent with the finding that there is only weak secondary structure for $[Cu(\mathbf{L1})(H_2O)(ClO_4)](ClO_4)$. The other three complexes have *M*-$[Cu(\mathbf{L2})]^{2+}$, *P*-$[Cu(\mathbf{L3})]^{2+}$, and *P*-$[Cu(\mathbf{L4})]^{2+}$ configurations (Figure 6), which is in line with the CD characterization.

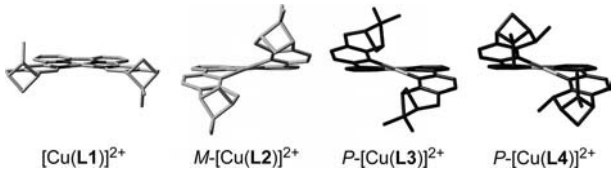

Figure 6. DFT simulated structures of $[Cu(\mathbf{L1})]^{2+}$, *M*-$[Cu(\mathbf{L2})]^{2+}$, *P*-$[Cu(\mathbf{L3})]^{2+}$, and *P*-$[Cu(\mathbf{L4})]^{2+}$.

Self-Assembly and Characterization of Double-Stranded Cu^{I}–qtpy Helicates

The first copper(I) complex of a chiral qtpy ligand was reported by Constable et al.[18] Using a similar procedure, chiral Cu^{I}–qtpy helicates of **L1**–**4** were prepared (Scheme 3). Mixing equimolar amounts of $[Cu(CH_3CN)_4](PF_6)$ and **L1**–**4** in degassed acetonitrile under a dinitrogen atmosphere instantly gave deep red solutions, which were stirred for 2 h. A large amount of diethyl ether was added to give dark red precipitates, which were collected by filtration and washed with diethyl ether to afford crude chiral Cu^{I}–qtpy helicates.

Elemental analyses of all the crude complexes show a Cu:L ratio of 1:1. ESI-MS support the formation of dinuclear complexes, $[Cu_2(\mathbf{L})_2](PF_6)_2$ (**L** = **L1**–**3**) and $[Cu_2(\mathbf{L4})_2](PF_6)_2$, which exhibit parent peaks $[M - PF_6]^+$ at *m*/*z* = 1269 and 1325, respectively. The isotopic patterns of the molecular ions are in good agreement with the theoretical calculations. Under high ionization energy, for $[Cu_2(\mathbf{L})_2]$-

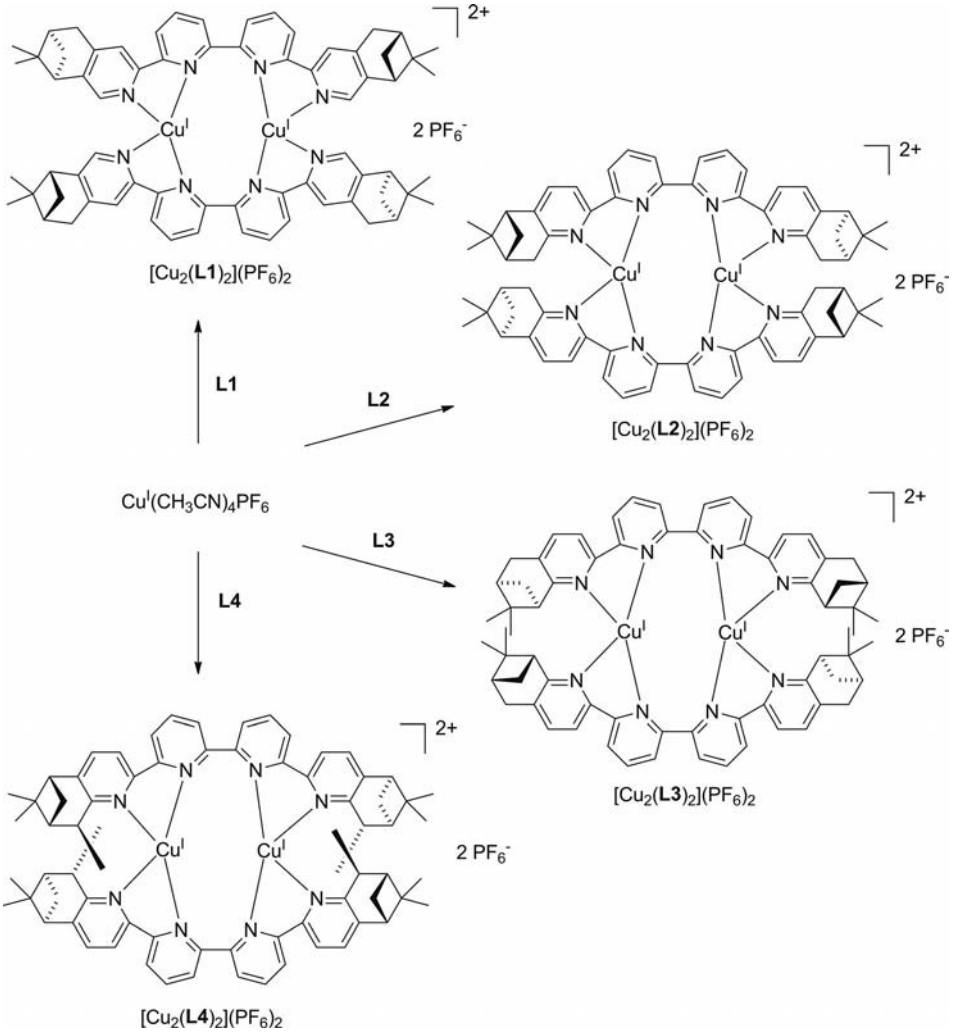

Scheme 3. Self-assembly of double-stranded Cu^{I} helicates with enantiopure **L1**–**4**.

$(PF_6)_2$ (**L** = **L1**–**3**) and $[Cu_2(\mathbf{L4})_2](PF_6)_2$, the doubly charged species $[M - 2PF_6]^{2+}$ is also observed at *m*/*z* = 561.6 and 589.9, respectively. Slow diffusion of diethyl ether into a methanol solution of $[Cu_2(\mathbf{L3})_2](PF_6)_2$ gave single crystals, which were suitable for X-ray analysis.

X-ray Structure of $[Cu_2(L3)_2](PF_6)_2$

The crystal structure of cationic $[Cu_2(\mathbf{L3})_2]^{2+}$ and the corresponding space-filling model are shown in Figure 7. Selected bond lengths and angles are summarized in Table 3. Each **L3** segments into two bipyridine domains and coordinates to Cu^{I} with a distorted tetrahedral geometry. The two ligand strands intertwine and, with the Cu ions positioned at the helical axis, form a double-helix with *P*-handedness. The bond angles and distances are within the typical range for similar $[Cu_2(qtpy)_2]^{2+}$ cations. The Cu–N distances vary from 1.991–2.115 Å. The Cu···Cu distance of 3.391 Å is slightly shorter than that for $[Cu_2(\mathbf{L2})_2](PF_6)_2$.[18b] The helical twist is largely achieved between the central rings of each ligand (48.16–49.05°), with smaller twists observed at the terminal rings (15.16–15.69°). With distances between the terminal and central pyridine rings of 3.726–4.189 Å, intrastrand π–π interaction probably plays an important role in stabilizing the double-helix structure.

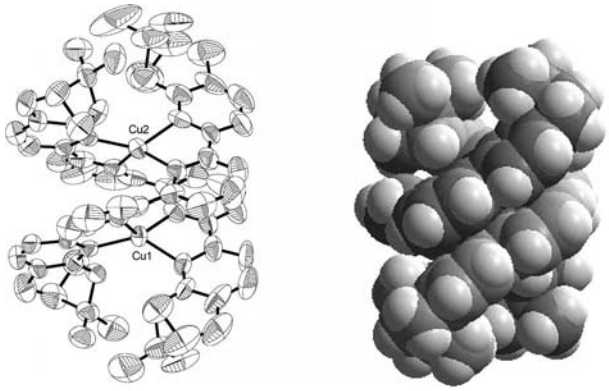

Figure 7. ORTEP drawing and space-filling model of *P*-$[Cu_2(\mathbf{L3})_2](PF_6)_2$. Thermal ellipsoids are drawn at 30% probability. Hydrogen atoms are omitted for clarity.

Table 3. Selected X-ray data for *P*-$[Cu_2(\mathbf{L3})_2](PF_6)_2$.

Selected distances [Å]		Selected angles [°]	
Cu1–N1	1.991(3)	N1–C12–C13–N2	15.2(4)
Cu1–N2	2.103(4)	N2–C17–C18–N3	48.2(6)
Cu2–N3	2.039(4)	N3–C22–C23–N4	15.7(6)
Cu2–N4	2.065(4)	overall helical twist of the first ligand strand	79.01
Cu1–N5	2.054(3)	N5–C46–C47–N6	15.6(6)
Cu1–N6	2.026(4)	N6–C51–C52–N7	49.1(6)
Cu2–N7	2.115(4)	N7–C56–C57–N8	15.6(7)
Cu2–N8	2.004(3)	overall helical twist of the second ligand strand	80.21
Cu1–Cu2	3.391(1)		

^{1}H NMR Spectroscopic Studies

The solution behavior of double-stranded dinuclear $[Cu_2(\mathbf{L})_2](PF_6)_2$ (**L** = **L1**–**4**) was characterized by NMR spectroscopy in $CDCl_3$. As only half of the ligand resonances are observed from the ^{1}H and ^{13}C NMR spectra, all show a twofold symmetry. In the aromatic region (7–9 ppm) of the ^{1}H NMR spectra, crude $[Cu_2(\mathbf{L})_2](PF_6)_2$ (**L** = **L1**–**3**) show both a major and a minor set of resonances, whereas $[Cu_2(\mathbf{L4})_2](PF_6)_2$ shows only one set (Figure 8). Following gCOSY ^{1}H–^{1}H NMR experiments, the proton resonances of all complexes were assigned. The two sets of resonances are correlated to the *P*/*M* diastereomers of the double helicates. The ratios of the diastereomers were assigned by pairs of CH_3 protons on the chiral substituents of the complexes, which show large peak shifts to *P* or *M* helical chirality. The diastereomeric ratios of the helicates indicate the influence of the chiral substituent of the ligand on the selectivity of *P* and *M* helicity. $[Cu_2(\mathbf{L1})_2](PF_6)_2$ showed the lowest diastereomeric excess (*de*) (52%), whereas a single diastereomer was observed for $[Cu_2(\mathbf{L4})_2](PF_6)_2$ (≥ 95%). The *de* values of $[Cu_2(\mathbf{L2})_2](PF_6)_2$ and $[Cu_2(\mathbf{L3})_2](PF_6)_2$ were 64 and 71% respectively. The *de* of crude $[Cu_2(\mathbf{L2})_2](PF_6)_2$ obtained here is much lower than that observed by Constable in previous studies (*de* > 97.5%).[18b] Although the procedure we employed for complexation is similar to Constable's, it differs in the use of $[NH_4][PF_6]$ in precipitation, which may account for the difference in *de*.

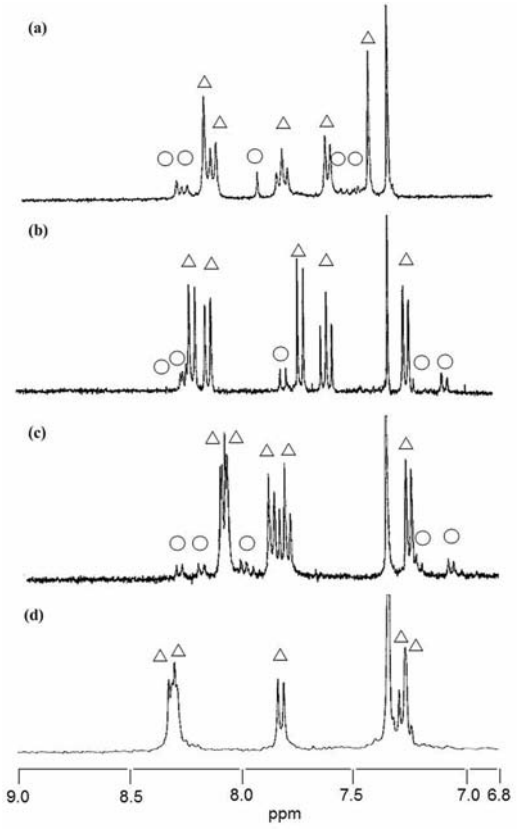

Figure 8. Aromatic region (6.8–9.0 ppm) of the ^{1}H NMR spectra (300 MHz) of crude dinuclear Cu^I double helicates for (a) **L1**, (b) **L2**, (c) **L3**, and (d) **L4** (Δ: major diastereomer; ○: minor diastereomer).

CD Characterization of Cu^I–qtpy Complexes

The helical structure of crude $[Cu_2(\mathbf{L})_2](PF_6)_2$ (**L** = **L1**–**4**) in solution was studied by CD spectroscopy. The diastereomeric mixtures were measured in CH_2Cl_2 at room temperature (Figure 9). The strong sinoidal absorptions (Cotton effect) in the region 320–350 nm can be attributed to ligand-centered π–π* transitions. The helicates display additional weak bands at 460 nm, which is coincident with a metal-to-ligand absorption. The Cotton effect has been used in the assignment of chirality of helicates in solution.[18,23] As in Constable's previous studies on $[Cu_2(\mathbf{L2})_2](PF_6)_2$,[18] the negative absorption (Cotton effect) at 320 nm is assigned to *M*-handedness. For $[Cu_2(\mathbf{L3})_2](PF_6)_2$, the positive absorption at 320 nm is assigned to *P*-handedness, which is consistent with our solid-state characterization. These two examples demonstrate good correlation between solid-state and solution CD characterizations. In addition, time-dependent (TD)-DFT calculations of the CD spectrum of $[Cu_2(\mathbf{L3})_2](PF_6)_2$ indicate that the CD signals are dominated by internuclear exciton coupling, which confirms the experimental result (see Supporting Information, Figures S1 and S2). Thus, based on the CD signals, we can

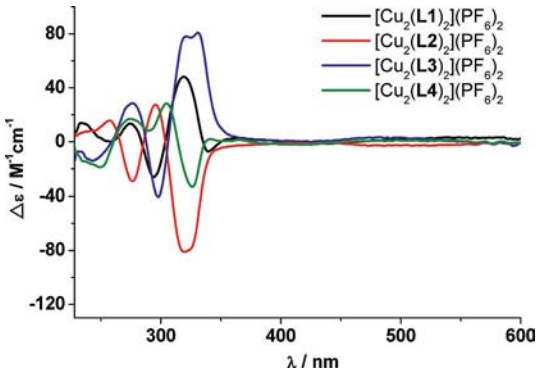

Figure 9. CD spectra of crude $[Cu_2(\mathbf{L})_2](PF_6)_2$ (**L** = **L1**–**4**) in CH_2Cl_2 solution.

assign the major diastereomers of $[Cu_2(\mathbf{L1})_2](PF_6)_2$ as *P*-handed, whereas that of $[Cu_2(\mathbf{L4})_2](PF_6)_2$ has *M*-handedness.

Stereoselectivity and Molecular Structures of Cu^I–qtpy Helicates

In the double-stranded dinuclear Cu^I helicates, the chiral qtpy ligand induces significant diastereoselectivity, which is complete for **L4**. The geometries of the four pairs of diastereomers have been fully optimized by DFT (see detailed geometries in the Supporting Information), and Figure 10 depicts the four major diastereomers. Table 4 summarizes the energy difference between the major and minor diastereomer pairs, defined as $E_{major} - E_{minor}$ and the steric energy between the ligand strands is defined as $E_{helicate\ without\ Cu} - (E_{strand\ A} + E_{strand\ B})$ with counterpoise correction. It should be noted that the major diastereomers are not always of lower energy than their corresponding minor diastereomers, which suggests that the formation of diastereomers may be a kinetically controlled reaction. Also, as the steric interaction energies are all positive values, the interactions between the strands are dominated by repulsive interactions. The minor diastereomers do not always have lower interaction energies, which suggests that we cannot use the interaction between the qtpy strands as the only factor to account for the selectivity between the two diastereomers. It should be noted that the stability of the helicates is not solely determined by the repulsion between the qtpy strands but is also a result of the interplay of (1) the stability of the $[CuN_4]$ core, (2) electrostatic interactions between the charged Cu^+ ions, and (3) solvent stabilization. For example, M-$[Cu_2(\mathbf{L1})_2]^{2+}$ has a smaller interstrand repulsion than P-$[Cu_2(\mathbf{L1})_2]^{2+}$ but it is overall slightly less stable than P-$[Cu_2(\mathbf{L1})_2]^{2+}$.

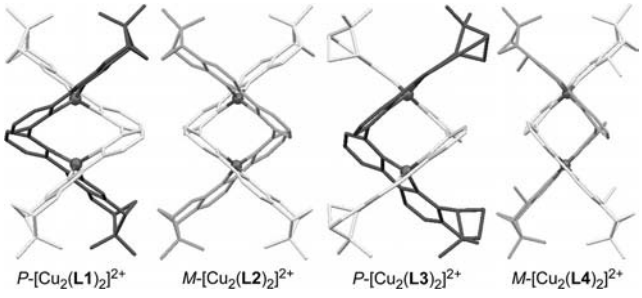

Figure 10. Double-stranded dinuclear Cu^I helicates P-$[Cu_2(\mathbf{L1})_2]^{2+}$, M-$[Cu_2(\mathbf{L2})_2]^{2+}$, P-$[Cu_2(\mathbf{L3})_2]^{2+}$, and M-$[Cu_2(\mathbf{L4})_2]^{2+}$ fully optimized by DFT.

Cu^I Helicate of L1m

$[Cu_2(\mathbf{L1m})_2](PF_6)_2$ was prepared using the same conditions shown in Scheme 3. It was isolated and characterized by elemental analysis and ESI-MS. However, the complexity of the ^1H NMR spectrum suggested that there was more than one isomer in the solution. Following a gCOSY ^1H–^1H NMR experiment and careful assignment based on the number of resonances and integrations (Figure 11), two directional isomers, head-to-head *HH*-$[Cu_2(\mathbf{L1m})_2](PF_6)_2$ and

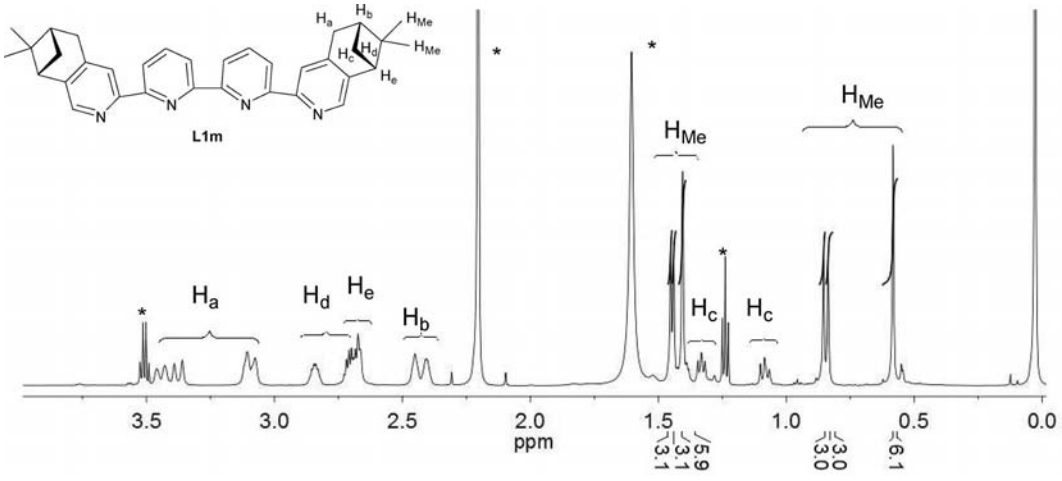

Figure 11. Aliphatic region of 600 MHz ^1H NMR spectra (600 MHz, $CDCl_3$) of crude $[Cu_2(\mathbf{L1m})_2](PF_6)_2$. The peaks marked with an asterisk are arisen from solvent.

Table 4. Energies [kcal mol^{-1}] of the diastereomers fully optimized by DFT.

Complex	$E_{major} - E_{minor}$	$E_{helicate\ without\ Cu} - (E_{strand\ A} + E_{strand\ B})$		Cu···Cu distance [Å]	
		Major	Minor	Major	Minor
$[Cu_2(\mathbf{L1})_2]^{2+}$	–0.007	24.15	23.77	3.093	3.189
$[Cu_2(\mathbf{L2})_2]^{2+}$	0.884	21.39	19.63	3.540	5.031
$[Cu_2(\mathbf{L3})_2]^{2+}$	2.582	22.31	19.23	3.547	5.060
$[Cu_2(\mathbf{L4})_2]^{2+}$	–6.946	20.01	23.95	5.157	3.492

head-to-tail *HT*-[Cu_2(**L1m**)$_2$](PF_6)$_2$ were assigned. The assignment was based on the rationalization that the opposite helical chiral isomers of each directional isomer are enantiomers and cannot be distinguished by ^{1}H NMR spectroscopy. The symmetry of [Cu_2(**L1m**)$_2$](PF_6)$_2$ is reduced from D_2 to C_2 compared to [Cu_2(**L1**)$_2$](PF_6)$_2$. The methyl hydrogen atoms, H_{Me}, on the two chiral subsitutents of the ligand are no longer equivalent, which give four singlet signals of the same integration for each directional isomer. Although some of the H_{Me} signals overlap, the integrations still suggest that there is no significant preference between the two directional isomers.

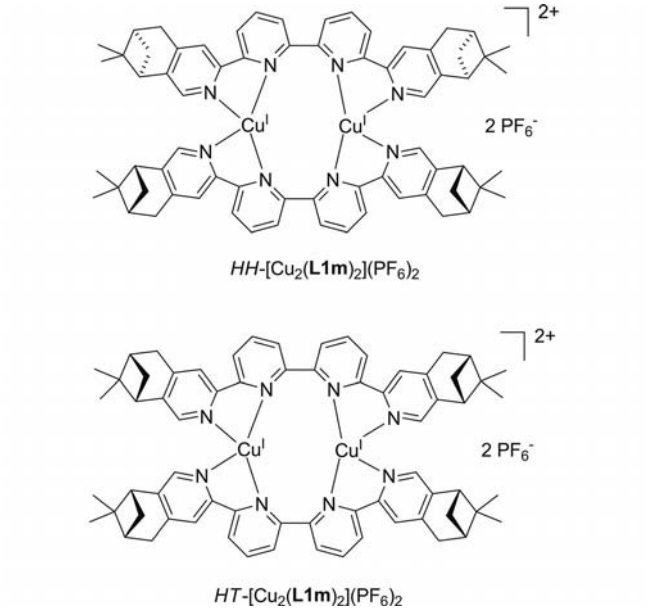

Formation of the Heterostrand Cu^I–qtpy Helicates

Heterostrand Cu^I–qtpy helicates are formed if two different chiral qtpy ligands are involved in the self-assembly process. The formation of these helicates was studied by reactions involving **L1**–**L3** with **L4**. Because of the mass differences between the ligands, the reactions were monitored by ESI-MS. The crude products were isolated in the same way as the other helicates and their mass spectra were measured. All the spectra show signals indicating the presence of [Cu_2(**L**)(**L4**)](PF_6)$_2$ (**L** = **L1**–**L3**) heterostrand helicates (Figure 12). However, the intensity of the signals suggests that different ratios of the homo- and heterostrand helicates are formed with different ligands. In an ideal case, the homo- and heterostrand helicates would have a 1:1 ratio if the formation follows a statistical distribution. Any ratio that deviates from this suggests a selectivity preference towards the formation of either homo- or heterostrand helicates. The higher ratio of the homo- to the heterostrand helicate (3.7:1 for **L1** and **L4**, 3.7:1 for **L2** and **L4**, 2.6:1 for **L3** and **L4**) suggests that there is always a preference towards the homostrand helicates irrespective of their chirality preference.

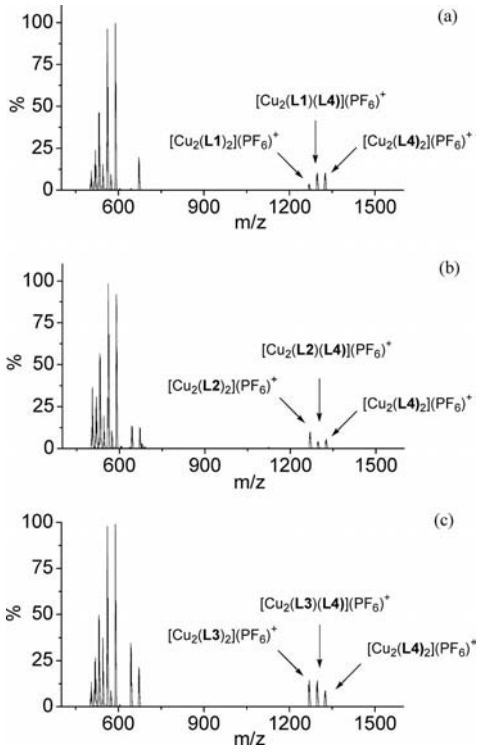

Figure 12. ESI-MS of mixtures of homo- and heterostrand helicates (a) **L1** and **L4**, (b) **L2** and **L4**, and (c) **L3** and **L4**.

Discussion

The helix formation of a mononuclear Cu^{II} complex is governed by the strong steric interaction between the chiral groups of the terminal pyridine units of the qtpy ligand. Although having the same chiral centers, [4,5]-substituted **L1** does not induce significant helical distortion in [Cu(**L1**)-(H_2O)(ClO_4)](ClO_4), whereas [5,6]-substituted **L3** induces a significant helical distortion of [Cu(**L3**)(ClO_4)$_2$]. Although no crystal structures were obtained for the Cu^{II} complexes of [5,6]-substituted **L2** and **L4**, their helical nature was confirmed by CD and UV spectroscopy.

For the mononuclear Cu^{II} complexes of [5,6]-substituted ligands **L2**–**4**, ^{1}H NMR spectra gave one set of broad signals and large CD absorptions were observed, which suggests high stereoselectivity. Molecular modeling, which shows helix formation induced by avoidance of steric interactions, further strengthens the observation. Helix formation of opposite handedness is not favored. All the observations and experimental data support the stereoselective formation of single-stranded mononuclear helical complexes. Thus, the handedness of Cu^{II} helical complexes can be controlled and predetermined by the chiral groups. The bulky dimethyl groups of the pinene rings of **L2** face in the opposite direction to those of **L3**, and *M*-[Cu(**L2**)(ClO_4)$_2$] and *P*-[Cu(**L3**)(ClO_4)$_2$] are formed from these ligands, respectively. Interestingly, as observed from the opposing sign in the CD absorption compared to that of **L2**, **L4**, which contains a

methyl group on the lower side of the four-membered pinene ring of **L2**, switches the chirality of Cu^{II} complex from *M* to *P*.

Upon coordination to tetrahedral Cu^{I} ions, all the chiral qtpy ligands induce a double helix structure by twisting the bipyridine domains between two Cu^{I} ions with the integrity maintained by multiple intramolecular π–π stacking. In contrast to the mononuclear Cu^{II} complexes, the stereoselective formation of double-stranded helicates requires complementary matching of the two ligands. Constable and coworkers have previously proposed that the distance between the chiral groups of one ligand strand and the central pyridine ring of the other ligand strand is the major determining factor for the diastereoselectivity of the double-stranded helicate. We found that, except for **L4**, the interaction energies between the qtpy strands are higher for the major diastereomers than for their corresponding minor diastereomers from DFT calculations. These results suggest that the formation of the diastereomers is a kinetically controlled reaction.

The handedness of Cu^{I} helicates is again dictated by the chiral centers of the ligands. As an example, in *P*-$[Cu_2(\mathbf{L3})_2](PF_6)_2$, **L3** induces a λ,λ configuration on the metal center, which gives rise to a *P* helix as the major diastereomer, whereas **L2** induces a Δ,Δ configuration on the metal center, which gives rise to an *M* helix as the major diastereomer of $[Cu_2(\mathbf{L2})_2](PF_6)_2$. In this sense, the absolute configuration of the Cu^{I} center is predetermined by the ligand and the configuration of the well-defined chiral helix follows. Accordingly, **L1** and **L3** will give *P* helices, whereas **L2** and **L4** will give *M* helices as the major diastereomers. An interesting point to note is that **L1**, which is almost planar in its Cu^{II} complex, forms a helical Cu^{I} complex with a large CD signal. This difference could act as a two read-out signals, which could be useful in molecular machinery.

Conclusions

Two series of chiral helical copper complexes, single-stranded mononuclear complexes and double-stranded dinuclear helicates, were formed with qtpy ligands. The helical formation and stereoselectivity of the helicates were correlated through X-ray crystallographic, NMR spectroscopic, circular dichroism, and modeling studies. In the single-stranded mononuclear complexes, the steric interaction between the two chiral auxiliaries of the ligand was shown to be a key factor in influencing stereoselectivity. For the dinuclear double-stranded Cu^{I} helicate, DFT calculations suggested that interactions between the chiral groups of the ligand strands in the helicate are not responsible for determining the helical chirality of the Cu^{I} complexes. Complete diastereoselective formation of a double-stranded helicate is achieved with **L4**. Further development of helical complexes with other metal ions and application of these helical copper complexes in asymmetric catalysis are under active investigation.

Experimental Section

Caution: Perchlorate salts of organic cations are potentially explosive and should be handled with great care.

Chemicals and Starting Materials: All air-sensitive manipulations were carried out under an atmosphere of dry dinitrogen. The solvents used for synthesis were of analytical grade. Dichloromethane and acetonitrile were distilled under dinitrogen with calcium hydride. All starting chemicals were of reagent-grade quality, obtained commercially, and used as received without further purification.

Physical Measurements and Instrumentation: Infrared spectra in the range 500–4000 cm^{-1} as KBr plates were recorded with a Perkin–Elmer Model FTIR-1600 spectrometer. UV/Vis spectra were measured with a Hewlett–Packard 8452A ultraviolet visible diode array spectrophotometer. ^1H and ^{13}C NMR spectra were recorded with a Varian YH300 300 MHz NMR spectrometer. The ^1H chemical shift was referenced to tetramethylsilane. ESI-MS were measured with a PE SCIEX API 365 LC-MS/MS system. Elemental analyses were performed with a Vario EL elemental analyzer. CD spectra were recorded with a Jasco J-715 spectropolarimeter with a 0.1 cm cell at 25 °C, and the results were given in $\Delta\varepsilon$ ($M^{-1}\,cm^{-1}$).

Crystal Structure Determination: Crystallographic data for **L1**, $[Cu(\mathbf{L1})(H_2O)(ClO_4)](ClO_4)$, $[Cu(\mathbf{L1m})(ClO_4)(H_2O)](ClO_4)$, $[Cu(\mathbf{L3})(ClO_4)_2]$, and $[Cu_2(\mathbf{L3})_2](PF_6)_2$ are tabulated in Table 5. Intensity data were collected at 293 K with a Bruker Axs SMART 1000 CCD area detector using graphite-monochromated Mo-K_α radiation (λ = 0.71073 Å). All collected frames were processed with the SAINT software, and absorption correction was applied (SADABS) to the collected reflections. The structures were solved by direct methods (SHELXTL) in conjunction with standard difference Fourier syntheses. All non-hydrogen atoms were assigned with anisotropic displacement parameters. The hydrogen atoms were generated in their idealized positions and allowed to ride on the respective carbon atoms.

CCDC-776974 (for **L1**), -776975 {for $[Cu(\mathbf{L1})(H_2O)(ClO_4)](ClO_4)$}, -776976 {for $[Cu(\mathbf{L1m})(ClO_4)(H_2O)](ClO_4)$}, -776977 {for $[Cu(\mathbf{L3})(ClO_4)_2]$}, and -776978 {for $[Cu_2(\mathbf{L3})_2](PF_6)_2$} contain the supplementary crystallographic data for this paper. These data can be obtained free of charge from The Cambridge Crystallographic Data Centre via www.ccdc.cam.ac.uk/data_request/cif.

General Procedure for Purification of Chiral qtpy Ligands: The crude qtpy ligand was acidified with 6 N HCl (2 mL). The protonated ligand was dissolved in the minimum amount of methanol and isolated by precipitation with diethyl ether. The pale yellow solid was recrystallized from methanol, collected by filtration, and washed twice with cold methanol. It was then neutralized with 2 M sodium hydroxide and extracted into CH_2Cl_2. The organic layer was washed with deionized water and the solvent was removed under reduced pressure.

General Method for Preparation of Mononuclear Single-Stranded Cu^{II}–qtpy Complexes: An ethanol solution (5 mL) of hydrated $Cu(ClO_4)_2$ (0.2 mmol, 34 mg) was added to a solution of the appropriate ligand (0.2 mmol) in CH_2Cl_2 (5 mL). A blue solution formed immediately, and the reaction mixture was stirred for 2 h at ambient temperature. The solvent was removed under vacuum. The resulting solid was washed several times with diethyl ether and recrystallized by slow evaporation of a concentrated ethanol solution.

$[Cu(L1)(H_2O)(ClO_4)](ClO_4)$: Blue solid; yield 145 mg (90%). IR (KBr): $\tilde{\nu}$ = 3467 (bm), 2924 (m), 1603 (m), 1577 (m), 1470 (s), 1316 (m), 1096 (vs), 619 (m) cm^{-1}. UV/Vis (CH_2Cl_2, 2.5×10^{-5} M): λ_{max}

Table 5. X-ray data for **L1**, [Cu(**L1**)(H_2O)(ClO_4)](ClO_4), [Cu(**L1m**)(H_2O)(ClO_4)](ClO_4), [Cu(**L3**)(ClO_4)$_2$], and [Cu_2(**L3**)$_2$](PF_6)$_2$.

	L1	[Cu(**L1**)(H_2O)(ClO_4)](ClO_4)	[Cu(**L1m**)(H_2O)(ClO_4)](ClO_4)	[Cu(**L3**)(ClO_4)$_2$]	[Cu_2(**L3**)$_2$](PF_6)$_2$
Formula	$C_{34}H_{34}N_4$	$C_{34}H_{36}Cl_2CuN_4O_9$	$C_{34}H_{36}Cl_2CuN_4O_9$	$C_{35}H_{38}Cl_2CuN_4O_9$	$C_{72}H_{78}Cu_2F_{12}N_8OP_2$
Formula weight	498.65	779.11	777.09	793.13	1488.44
Crystal color, habit	colorless, block	green, block	green, block	green, rod	red, block
Crystal dimensions	0.30 × 0.25 × 0.15 mm	0.28 × 0.22 × 0.20 mm	0.22 × 0.14 × 0.12 mm	0.32 × 0.16 × 0.13 mm	0.29 × 0.25 × 0.2 mm
Crystal system	monoclinic	triclinic	triclinic	orthorhombic	orthorhombic
Lattice type	primitive	primitive	primitive	primitive	primitive
Lattice parameters	*a* = 6.683(1) Å, *b* = 17.785(2) Å, *c* = 23.459(2) Å, *α* = 90.00°, *β* = 90.128(1)°, *γ* = 90.00°, *V* = 2788.5(3) Å^3	*a* = 7.7672(4) Å, *b* = 15.192(8) Å, *c* = 15.4805(8) Å, *α* = 78.216(1)°, *β* = 88.252(1)°, *γ* = 81.894(1)°, *V* = 1770.3(2) Å^3	*a* = 7.7739(5) Å, *b* = 15.206(1) Å, *c* = 15.481(1) Å, *α* = 78.234(1)°, *β* = 88.283(1)°, *γ* = 81.932(1)°, *V* = 1773.8(2) Å^3	*a* = 12.380(2) Å, *b* = 15.633(3) Å, *c* = 19.013(3) Å, *α* = 90.00°, *β* = 90.00°, *γ* = 90.00°, *V* = 3679.9(10) Å^3	*a* = 14.964(1) Å, *b* = 19.520(1) Å, *c* = 24.562(2) Å, *α* = 90.00°, *β* = 90.00°, *γ* = 90.00°, *V* = 7174.5(8) Å^3
Space group	$P2_1$	$P\bar{1}$	$P\bar{1}$	$P2_12_12_1$	$P2_12_12_1$
Z	4	2	2	4	4
D_{calc}	1.188 Mg/m^3	1.462 Mg/m^3	1.455 Mg/m^3	1.432 Mg/m^3	1.378 Mg/m^3
Temperature	273(2) K	273(2) K	273(2) K	293(2) K	293(2) K
Radiation	Mo-K_α (*λ* = 0.71073 Å)	Mo-K_α (*λ* = 0.71073 Å)	Mo-K_α (*λ* = 0.71073 Å)	Mo-K_α (*λ* = 0.71073 Å)	Mo-K_α (*λ* = 0.71073 Å)
μ(Mo-K_α)	0.070 mm^{-1}	0.827 mm^{-1}	0.825 mm^{-1}	0.797 mm^{-1}	0.717 mm^{-1}
$2\theta_{max}$	56.62°	56.50°	50.00°	50.00°	50.00°
F(000)	1064	806	802	1644	3080
Reflections collected/unique	16594/9226 (R_{int} = 0.0394)	10555/9092 (R_{int} = 0.0151)	8826/7385 (R_{int} = 0.0154)	18227/6428 (R_{int} = 0.0392)	35403/12574 (R_{int} = 0.073)
Absolute structure parameter	–	0.03(1)	0.26(2)	–0.02(2)	0.00(2)
R indices [$I > 2\sigma(I)$]	R_1 = 0.0509, wR_2 = 0.1133	R_1 = 0.0457, wR_2 = 0.1255	R_1 = 0.053, wR_2 = 0.1475	R_1 = 0.0481, wR_2 = 0.1191	R_1 = 0.0598, wR_2 = 0.1373
R indices (all data)	R_1 = 0.1284, wR_2 = 0.1425	R_1 = 0.0607, wR_2 = 0.137	R_1 = 0.0663, wR_2 = 0.1602	R_1 = 0.0784, wR_2 = 0.1371	R_1 = 0.1479, wR_2 = 0.1792

(ε_{max}) = 315 (22.5 × 10^3), 349 (11.2 × 10^3), 363 (11.1 × 10^3), 640 (1.5 × 10^2) nm. ESI-MS: *m*/*z* = 281 [Cu(**L1**)]$^{2+}$, 660 [Cu(**L1**)(ClO_4)]$^+$. [Cu(**L1**)(H_2O)(ClO_4)](ClO_4) (779.12): calcd. C 52.41, H 4.67, N 7.19; found C 52.70, H 4.74, N 7.24.

[Cu(L2)(ClO_4)$_2$]: Green solid; yield 140 mg (92%). IR (KBr): $\tilde{\nu}$ = 3431 (bm), 2924 (m), 1577 (m), 1475 (m), 1091 (vs), 804 (m), 619 (m) cm^{-1}. UV/Vis (CH_2Cl_2, 2.5 × 10^{-5} M): λ_{max} (ε_{max}) = 321 (18.8 × 10^3), 354 (10.3 × 10^3), 730 (1.4 × 10^2) nm. ESI-MS: *m*/*z* = 281 [Cu**L2**]$^{2+}$, 660 [Cu(**L2**)(ClO_4)]$^+$. [Cu(**L2**)(ClO_4)$_2$] (761.11): calcd. C 53.65, H 4.51, N 7.36; found C 52.95, H 4.47, N 7.34.

[Cu(L3)(ClO_4)$_2$]: Green solid; yield 145 mg (95%). IR (KBr): $\tilde{\nu}$ = 3436 (bm), 2929 (m), 1572 (m), 1254 (m), 1106 (vs), 799 (m), 620 (m) cm^{-1}. UV/Vis (CH_2Cl_2, 2.5 × 10^{-5} M): λ_{max} (ε_{max}) = 325 (25.6 × 10^3), 356 (10.3 × 10^3), 369 (9.1 × 10^3), 764 (1.2 × 10^2) nm. ESI-MS: *m*/*z* = 281 [Cu(**L3**)]$^{2+}$, 660 [Cu(**L3**)(ClO_4)]$^+$. [Cu(**L3**)(ClO_4)$_2$] (761.11): calcd. C 53.65, H 4.51, N 7.36; found C 52.84, H 4.48, N 7.33.

[Cu(L4)(ClO_4)$_2$]: Deep green solid; yield 140 mg (92%). IR (KBr): $\tilde{\nu}$ = 3452 (bm), 2965 (m), 2924 (m), 1567 (m), 1424 (m), 1239 (m), 1086 (vs), 804 (m), 788 (m), 619 (m) cm^{-1}. UV/Vis (CH_2Cl_2, 2.5 × 10^{-5} M): λ_{max} (ε_{max}) = 306 (27.3 × 10^3), 354 (16.8 × 10^3), 759 (8.0 × 10) nm. ESI-MS: *m*/*z* = 295 [Cu(**L4**)]$^{2+}$, 689 [Cu(**L4**)(ClO_4)]$^+$. [Cu(**L4**)(ClO_4)$_2$]·Et_2O (863.28): calcd. C 55.64, H 5.62, N 6.49; found C 55.32, H 5.57, N 6.43.

General Method for Preparation of Dinuclear Double-Stranded Cu^I–qtpy Helicates: [Cu(MeCN)$_4$][PF_6] (0.2 mmol, 42 mg) was treated with the appropriate ligand (0.2 mmol) in degassed CH_3CN (2 mL). Dark red solutions were formed immediately and the reaction mixture was stirred for 2 h at ambient temperature. Any solids were removed by filtration through Celite. The solvent was then removed under vacuum.

[Cu_2(L1)$_2$][PF_6]$_2$: Dark red crystals; yield 139 mg (95%). IR (KBr): $\tilde{\nu}$ = 2930 (m), 1598 (m), 1465 (m), 1102 (s) cm^{-1}. UV/Vis (CH_2Cl_2, 1.53 × 10^{-4} M): λ_{max} (ε_{max}) = 269 (50300), 292 (45300), 428 (5650), 520 (2743) nm. ESI-MS: *m*/*z* = 1269 [Cu_2(**L1**)$_2$][PF_6]$^{1+}$. [Cu_2(**L1**)$_2$][PF_6]$_2$ (1414.34): calcd. C 56.79, H 4.97, N 8.02; found C 56.07, H 4.86, N 7.75.

[Cu_2(L2)$_2$][PF_6]$_2$: Dark red crystals; yield 136 mg (96%). IR (KBr): $\tilde{\nu}$ = 2929 (m), 1557 (m), 1434 (m), 1075 (m), 840 (vs), 558 (m) cm^{-1}. UV/Vis (CH_2Cl_2, 1.53 × 10^{-4} M): λ_{max} (ε_{max}) = 272 (69600), 311 (62700), 452 (11700), 548 (5000) nm. ESI-MS: *m*/*z* = 1269 [Cu_2(**L2**)$_2$][PF_6]$^+$. [Cu_2(**L2**)$_2$][PF_6]$_2$ (1414.34): calcd. C 56.79, H 4.97, N 8.02; found C 57.02, H 5.02, N 7.90.

[Cu_2(L3)$_2$][PF_6]$_2$: Dark red crystals; yield 127 mg (90%). IR (KBr): $\tilde{\nu}$ = 2925 (m), 1567 (m), 1424 (m), 1260 (m), 1076 (m), 843 (vs), 554 (m) cm^{-1}. UV/Vis (CH_2Cl_2, 1.53 × 10^{-4} M): λ_{max} (ε_{max}) = 264 (40.8 × 10^3), 304 (45.3 × 10^3), 423 (6.4 × 10^3), 545 (2.8 × 10^3) nm. ESI-MS: *m*/*z* = 1269 [Cu_2(**L3**)$_2$][PF_6]$^+$. [Cu_2(**L3**)$_2$][PF_6]$_2$ (1414.34): calcd. C 56.79, H 4.97, N 8.02; found C 56.53, H 5.03, N 7.80.

[Cu_2(L4)$_2$][PF_6]$_2$: Dark red crystals; yield 130 mg (92%). IR (KBr): $\tilde{\nu}$ = 2919 (m), 1557 (m), 1424 (m), 1085 (s), 840 (vs), 553 (m) cm^{-1}. UV/Vis (CH_2Cl_2, 1.53 × 10^{-4} M): λ_{max} (ε_{max}) = 272 (25.2 × 10^3), 320 (25.0 × 10^3), 427 (7.4 × 10^3), 523 (2.4 × 10^3) nm. ESI-MS: *m*/*z* = 1324 [Cu_2(**L4**)$_2$][PF_6]$^+$. [Cu_2(**L4**)$_2$][PF_6]$_2$ (1470.45): calcd. C 57.27, H 5.37, N 7.75; found C 58.09, H 5.29, N 7.53.

[Cu_2(L1m)$_2$][PF_6]$_2$: Yield: 126 mg (89%). ESI-MS: *m*/*z* = 1269 [Cu_2(**L1m**)$_2$][PF_6]$^{1+}$. [Cu_2(**L1m**)$_2$][PF_6]$_2$·2.5H_2O (1459.38): calcd. C 55.96, H 5.04, N 7.68; found C 55.81, H 4.95, N 7.70.

DFT Calculations: DFT calculations were employed to investigate the geometry of the complexes and their UV and CD spectra. Their electronic ground states were optimized without symmetry constrains using the density functional PBE1PBE,[27] which is a hybrid of the Perdew, Burke, and Ernzerhof exchange and correlation functional and 25% HF exchange. The Stuttgart small core relativistic effective core potentials were employed for Cu atoms with their accompanying basis sets.[28] The 6-31G basis set was employed for C, H, and N.[29] The electronic transitions for these complexes were calculated at the TD-DFT level using the same functional and basis sets. Tight self-consistent-field (SCF) convergence (10^{-8} au) was used for all calculations. All the DFT calculations were performed using the Gaussian 03 program package (revision D.01).[30] Although frequency calculation of the optimized geometry was hampered by the limitation of the computational power (the calculations involved too many basis functions and electrons, which were too large to be handled by our computers), the forces on the system were essentially zero and thus the optimized geometry was confirmed to be a stationary point.

Supporting Information (see footnote on the first page of this article): Details of the DFT calculations.

Acknowledgments

Financial support for this research project from the Research Grant council (GRF), Hong Kong (grant CityU 101108) and the City University of Hong Kong, SRG (grant CityU 7002607) are gratefully acknowledged.

[1] G. Seeber, B. E. F. Tiedemann, K. N. Raymond, *Top. Curr. Chem.* **2006**, *165*, 147.
[2] A. F. Williams, *Chem. Eur. J.* **1997**, *1*, 15.
[3] J.-M. Lehn, *Supramolecular Chemistry: Concepts and Perspectives*, Wiley-VCH, Weinheim, Germany, **1995**.
[4] E. C. Constable, in: *Comprehensive Supramolecular Chemistry*, vol. 9, *Polynuclear Transition Metal Helicates* (Ed.: J. P. Sauvage), Elsevier, Oxford, **1996**.
[5] a) M. Albrecht, *Chem. Rev.* **2001**, *101*, 3457; b) C. Piguet, G. Bernardinelli, G. Hopfgartner, *Chem. Rev.* **1997**, *97*, 2005.
[6] a) Y. Wang, H. Fu, F. Shen, X. Sheng, A. Peng, Z. Gu, H. Ma, J. S. Ma, J. Yao, *Inorg. Chem.* **2007**, *46*, 3548; b) J. Gregoliński, J. Lisowski, *Angew. Chem.* **2006**, *118*, 6268; *Angew. Chem. Int. Ed.* **2006**, *45*, 6122; c) D. F. Perkins, L. F. Lindoy, A. McAuley, G. V. Meehan, P. Turner, *Proc. Natl. Acad. Sci. USA* **2006**, *103*, 532.
[7] a) W. Zarges, J. Hall, J.-M. Lehn, C. Bolm, *Helv. Chim. Acta* **1991**, *74*, 1843; b) C. R. Woods, M. Benaglia, F. Cozzi, J. S. Siegel, *Angew. Chem.* **1996**, *108*, 1977; *Angew. Chem. Int. Ed. Engl.* **1996**, *35*, 1830; c) C. Provent, S. Hewage, G. Brand, G. Bernardinelli, L. J. Charbonnière, A. F. Williams, *Angew. Chem.* **1997**, *109*, 1346; *Angew. Chem. Int. Ed. Engl.* **1997**, *36*, 1287; d) O. Mamula, A. von Zelewsky, G. Bernardinelli, *Angew. Chem. Int. Ed.* **1998**, *37*, 290; e) M. A. Masood, E. J. Enemark, T. D. P. Stack, *Angew. Chem.* **1998**, *110*, 973; *Angew. Chem. Int. Ed.* **1998**, *37*, 928; f) U. Knof, A. von Zelewsky, *Angew. Chem.* **1999**, *111*, 312; *Angew. Chem. Int. Ed.* **1999**, *38*, 302; g) R. Prabaharan, N. C. Fletcher, M. Nieuwenhuyzen, *J. Chem. Soc., Dalton Trans.* **2002**, 602; h) O. Mamula, M. Lama, S. G. Telfer, A. Nakamura, R. Kuroda, H. Stoeckli-Evans, R. Scopelitti, *Angew. Chem.* **2005**, *117*, 2583; *Angew. Chem. Int. Ed.* **2005**, *44*, 2527; i) A. V. Wiznycia, J. Desper, C. J. Levy, *Chem. Commun.* **2005**, 4693; j) M. Albrecht, S. Dehn, G. Raabe, R. Fröhlich, *Chem. Commun.* **2005**, 5690; k) M. Albrecht, S. Mirtschin, M. De Groot, I. Janser, J. Runsink, G. Raabe, M. Kogej, C. A. Schalley, R. Fröhlich, *J. Am. Chem. Soc.* **2005**, *127*, 10371; l) J. Xu, K. N. Raymond, *Angew. Chem.* **2006**, *118*, 6630; *Angew. Chem. Int. Ed.* **2006**, *45*, 6480.
[8] a) K. Maruoka, N. Murase, H. Yamamoto, *J. Org. Chem.* **1993**, *58*, 2938; b) N. End, A. Pfaltz, *Chem. Commun.* **1998**, 589; c) N. End, L. Macko, Z. Margareta, A. Pfaltz, *Chem. Eur. J.* **1998**, *4*, 818; d) S. D. Dreher, T. J. Katz, K.-C. Lam, A. L. Rheingold, *J. Org. Chem.* **2000**, *65*, 815; e) Y.-Z. Zhu, Z.-P. Li, J.-A. Ma, F.-Y. Tang, L. Kang, Q.-L. Zhou, A. S. C. Chan, *Tetrahedron: Asymmetry* **2002**, *13*, 161; f) M. Seitz, A. Kaiser, D. R. Powell, A. S. Borovik, O. Reiser, *Adv. Synth. Catal.* **2004**, *346*, 737; g) T. Hasegawa, Y. Furusho, H. Katagiri, E. Yashima, *Angew. Chem.* **2007**, *119*, 5989; *Angew. Chem. Int. Ed.* **2007**, *46*, 5885.
[9] a) M. J. Hannon, V. Moreno, M. J. Prieto, E. Moldrheim, E. Sletten, I. Meistermann, C. J. Isaac, K. J. Sanders, A. Rodger, *Angew. Chem. Int. Ed.* **2001**, *40*, 880; b) A. C. G. Hotze, B. M. Kariuki, M. J. Hannon, *Angew. Chem.* **2006**, *118*, 4957; *Angew. Chem. Int. Ed.* **2006**, *45*, 4839.
[10] F. Cardinalli, H. Mamlouk, Y. Rio, N. Armaroli, J.-F. Nierengarten, *Chem. Commun.* **2004**, 1582.
[11] a) A. Bilyk, M. M. Harding, *J. Chem. Soc., Dalton Trans.* **1994**, 77; b) A. Bilyk, M. M. Harding, *J. Chem. Soc., Chem. Commun.* **1995**, 1697; c) G. Bokolinis, T. Riis-Johannessen, L. P. Harding, J. C. Jeffery, N. McLay, C. R. Rice, *Chem. Commun.* **2006**, 1980.
[12] a) J.-M. Lehn, J. P. Sauvage, J. Simon, R. Ziessel, C. Piccini-Leopardi, G.-P. Germain, M. Van Meersche, *Nouv. J. Chim.* **1983**, *7*, 413; b) J. P. Gisselbrecht, M. Gross, J.-M. Lehn, J. P. Sauvage, R. Ziessel, C. Piccinni-Leopardi, J. M. Arrieta, G. Germain, M. Van Meerssche, *Nouv. J. Chim.* **1984**, *8*, 661; c) A. Juris, S. Campagna, L. Bidd, J.-M. Lehn, R. Ziessel, *Inorg. Chem.* **1988**, *27*, 4007.
[13] a) E. C. Constable, S. M. Elder, J. Healy, M. D. Ward, D. A. Tocher, *J. Am. Chem. Soc.* **1990**, *112*, 4590; b) E. C. Constable, S. M. Elder, J. Healy, *J. Chem. Soc., Dalton Trans.* **1990**, 1669; c) E. C. Constable, S. M. Elder, D. A. Tocher, *Polyhedron* **1992**, *11*, 1337; d) E. C. Constable, S. M. Elder, D. A. Tocher, *Polyhedron* **1992**, *11*, 2599; e) E. C. Constable, M. J. Hannon, A. Martin, P. R. Raithby, D. A. Tocher, *Polyhedron* **1992**, *11*, 2967; f) E. C. Constable, S. M. Elder, M. J. Hannon, A. Martin, P. R. Raithby, D. A. Tocher, *J. Chem. Soc., Dalton Trans.* **1996**, 2423; g) E. C. Constable, M. J. Hannon, P. Harverson, M. Neuburger, D. R. Smith, V. F. Wanner, L. A. Whall, M. Zehnder, *Polyhedron* **2000**, *19*, 3276.
[14] a) K. T. Potts, K. A. Gheysen Raiford, M. Keshavarz-K, *J. Am. Chem. Soc.* **1993**, *115*, 2793; b) K. T. Potts, M. Keshavarz-K, F. S. Tham, H. D. Abruna, C. R. Arana, *Inorg. Chem.* **1993**, *32*, 4422; c) K. T. Potts, M. Keshavarz-K, F. S. Tham, H. D. Abruna, C. R. Arana, *Inorg. Chem.* **1993**, *32*, 4450.
[15] a) C.-W. Chan, C.-M. Che, M.-M. Cheng, Y. Wang, *Inorg. Chem.* **1992**, *31*, 4874; b) C.-M. Che, Y.-P. Wang, K.-S. Yeung, K.-Y. Wong, S.-M. Peng, *J. Chem. Soc., Dalton Trans.* **1992**, 2675; c) S.-M. Yang, K.-K. Cheung, C.-M. Che, *J. Chem. Soc., Dalton Trans.* **1993**, 3515; d) C.-W. Chan, C.-M. Che, S.-M. Peng, *Polyhedron* **1993**, *12*, 2169; e) C.-W. Chan, T.-F. Lai, C.-M. Che, *J. Chem. Soc., Dalton Trans.* **1994**, 895; f) C.-M. Che, C.-W. Chan, S.-M. Yang, C.-X. Guo, C.-Y. Lee, S.-M. Peng, *J. Chem. Soc., Dalton Trans.* **1995**, 2961; g) K.-M. Lam, K.-Y. Wong, S.-M. Yang, C.-M. Che, *J. Chem. Soc., Dalton Trans.* **1995**, 1103; h) X.-H. Li, L.-Z. Wu, C.-H. Tung, C.-M. Che, *Chem. Commun.* **2001**, 2280.
[16] D. B. Dell'Amico, F. Calderazzo, U. Englert, L. Labella, F. Marchetti, *J. Chem. Soc., Dalton Trans.* **2001**, 357.
[17] a) E. C. Constable, F. R. Heirtzler, M. Neuburger, M. Zehnder, *Chem. Commun.* **1996**, 933; b) E. C. Constable, F. R. Heirtzler, M. Neuburger, M. Zehnder, *J. Am. Chem. Soc.* **1997**, *119*, 5606.
[18] a) G. Baum, E. C. Constable, D. Fenske, T. Kulke, *Chem. Commun.* **1997**, 2043; b) E. C. Constable, T. Kulke, G. Baum, D. Fenske, *Inorg. Chem. Commun.* **1998**, *1*, 80; c) G. Baum, E. C. Constable, D. Fenske, C. E. Housecroft, T. Kulke, *Chem. Eur. J.* **1999**, *5*, 1862.

[19] a) V. Amendola, L. Fabbrizzi, L. Gianelli, C. Maggi, C. Mangano, P. Pallavicini, M. Zema, *Inorg. Chem.* **2001**, *40*, 3579; b) V. Amendola, M. Boiocchi, V. Brega, L. Fabbrizzi, L. Mosca, *Inorg. Chem.* **2010**, *49*, 997.
[20] a) L. Fabbrizzi, M. Licchelli, P. Pallavicini, *Acc. Chem. Res.* **1999**, *32*, 846; b) S. Zahn, J. W. Canary, *Science* **2000**, *288*, 1404; c) J. C. Jeffery, T. Riis-Johannessen, C. J. Anderson, C. J. Adams, A. Robinson, S. P. Argent, M. D. Ward, C. R. Rice, *Inorg. Chem.* **2007**, *46*, 2417.
[21] C.-T. Yeung, H.-L. Yeung, C.-S. Tsang, W.-Y. Wong, H.-L. Kwong, *Chem. Commun.* **2007**, 5203.
[22] H.-L. Kwong, H.-L. Yeung, W.-S. Lee, W.-T. Wong, *Chem. Commun.* **2006**, 4841.
[23] H.-L. Yeung, W.-Y. Wong, C.-Y. Wong, H.-L. Kwong, *Inorg. Chem.* **2009**, *48*, 4108.
[24] **L2** and $[Cu_2(\mathbf{L2})_2](PF_6)_2$ were first reported by Constable and coworkers in ref.[18b]
[25] a) M. Ziegler, A. von Zelewsky, *Coord. Chem. Rev.* **1998**, *177*, 257; b) N. Berova, K. Nakanishi, R. W. Woody (Eds.), *Circular Dichroism: Principles and Applications*, Wiley-VCH, New York, **2000**.
[26] S. G. Telfer, N. Tajima, N. R. Kuroda, *J. Am. Chem. Soc.* **2004**, *126*, 1408.
[27] a) J. P. Perdew, K. Burke, M. Ernzerhof, *Phys. Rev. Lett.* **1996**, *77*, 3865; b) C. Adamo, V. Barone, *J. Chem. Phys.* **1999**, *110*, 6158.
[28] M. Dolg, U. Wedig, H. Stoll, H. Preuss, *J. Chem. Phys.* **1978**, *86*, 866.
[29] W. J. Hehre, R. Ditchfield, J. A. Pople, *J. Chem. Phys.* **1972**, *56*, 2257.
[30] M. J. Frisch, G. W. Trucks, H. B. Schlegel, G. E. Scuseria, M. A. Robb, J. R. Cheeseman, J. A. Montgomery Jr., T. Vreven, K. N. Kudin, J. C. Burant, J. M. Millam, S. S. Iyengar, J. Tomasi, V. Barone, B. Mennucci, M. Cossi, G. Scalmani, N. Rega, G. A. Petersson, H. Nakatsuji, M. Hada, M. Ehara, K. Toyota, R. Fukuda, J. Hasegawa, M. Ishida, T. Nakajima, Y. Honda, O. Kitao, H. Nakai, M. Klene, X. Li, J. E. Knox, H. P. Hratchian, J. B. Cross, V. Bakken, C. Adamo, J. Jaramillo, R. Gomperts, R. E. Stratmann, O. Yazyev, A. J. Austin, R. Cammi, C. Pomelli, J. W. Ochterski, P. Y. Ayala, K. Morokuma, G. A. Voth, P. Salvador, J. J. Dannenberg, V. G. Zakrzewski, S. Dapprich, A. D. Daniels, M. C. Strain, O. Farkas, D. K. Malick, A. D. Rabuck, K. Raghavachari, J. B. Foresman, J. V. Ortiz, Q. Cui, A. G. Baboul, S. Clifford, J. Cioslowski, B. B. Stefanov, G. Liu, A. Liashenko, P. Piskorz, I. Komaromi, R. L. Martin, D. J. Fox, T. Keith, M. A. Al-Laham, C. Y. Peng, A. Nanayakkara, M. Challacombe, P. M. W. Gill, B. Johnson, W. Chen, M. W. Wong, C. Gonzalez, J. A. Pople, *Gaussian 03*, revision D.01, Gaussian, Inc., Wallingford, CT, **2004**.

Received: June 22, 2011
Published Online: October 12, 2011

